

Meris imageries to investigate surface chlorophyll in the upper gulf of Thailand

Anukul BURANAPRATHEPRAT^{1,2*}, K. Olaf NIEMANN², Satsuki MATSUMURA³ and Tetsuo YANAGI⁴

¹ Department of Aquatic Science, Faculty of Science, Burapha University, T. Saensuk, A. Muang, Chonburi 20131 Thailand

² Department of Geography, University of Victoria, PO Box 3050 STN CSC, Victoria, British Columbia V8W 3P5 Canada

³ Department of Marine Science, Chulalongkorn University, 254 Phayathai Rd., Bangkok 10330 Thailand

⁴ Research Institute for Applied Mechanics, Kyushu University, Kasuga, Fukuoka 816–8580 Japan

* E-mail: anukul@buu.ac.th

»» Received: 13 June 2008; Accepted 14 October 2008

Abstract—Medium Resolution Imaging Spectrometer Instrument (MERIS) Level 2 data were used to investigate the seasonal patterns of surface chlorophyll-a (chl-a) distribution related to eutrophic conditions in the upper Gulf of Thailand (UGoT). Initial overestimation of chl-a using MERIS R_{rs} was reduced when R_{rs} ratios were used. A local in-water algorithm, named Chula algorithm, was embedded into MERIS data due to higher accuracy in chl-a prediction, compared to standard MERIS chl-a products. Subsequent MERIS-derived chl-a maps revealed that during the northeast monsoon, high chl-a water moves westward, while during the southwest monsoon, it accumulates in the northeast corner of UGoT. These seasonal patterns of movement agree well with previous investigations on seasonal circulation and red tides in UGoT. Compared to other satellite data having larger spatial resolutions, MERIS chl-a images provide more details on chl-a distribution which may be useful for oceanographic studies in such a small coastal area as UGoT.

Key words: MERIS, chlorophyll distribution, Gulf of Thailand

Introduction

The upper Gulf of Thailand (UGoT) is located in the tropics at 13°N and 100°E. It is surrounded by land along the eastern, northern and western boundaries, and open to the central GoT in the south (Figure 1). The approximate area is 10⁴ km², and average and maximum depths are 15 m and 40 m respectively, with larger depths found in the east (Silpipat, 1987). Four main rivers—the Maeklong, the Thachin, the Chaopraya and the Bangpakong—discharge freshwater into the head of UGoT from west to east, respectively. The entire area is influenced by the two-inverse monsoon system; the northeast (November to January) and the southwest (May to August) monsoons. This monsoonal pattern is unique to Asia (Snidvongs 1998), and strong seasonal variations in prevailing wind over the area are common. The northeast winds bring cool and dry air from Siberia, while the west to southwest winds are characterized by moist and warm air from the Indian Ocean (Sojisuoporn 1994). However, heavy rain and tropical storms predominate when low pressure fronts migrate northward (May to June) and southward (August to November). Rainfall measured at Bangkok station in those phases could be as high as 400–500 mm a month while little to no precipitation falls in the dry period from December to February (data source: Thailand Meteorological Department). Seasonal variations in river discharges between wet

and dry seasons, therefore, become very large following major precipitation events.

Rapid development in areas bordering UGoT and population growth have resulted in pollution and deterioration of the quality of the marine environment. Mostly untreated waste waters from domestic and industrial sources are discharged directly into canals and main rivers (Cheevaporn and Menasveta 2003), and that drain into the Gulf. The most conspicuous and widespread impact on marine environment is eutrophication, resulting from very high loads of inorganic nutrients and an increased biological oxygen demand (BOD) (Chongprasith and Srinetr 1998). Such conditions are related to red tides in UGoT that usually occur in wet season during high river discharge events (Rungsupa 1997; Lirdwitayaprasit et al. 2006). The occurrence of red tides around UGoT were found to be related to monsoonal winds—along the western and the eastern coast during the northeast and the southwest wind influences, respectively (Lirdwitayaprasit et al. 1994).

The objective of this study was to investigate spatial distributions of chlorophyll-a (chl-a) at the sea surface, which, in UGoT, is used as a proxy for synoptically tracking phytoplankton patchiness or blooms. Fine spatial-resolution satellite images from the Medium Resolution Imaging Spectrometer Instrument (MERIS) were used for this purpose. MERIS data were also validated with the data, retrieved from field measurements, to examine their reliability for this study area,

which is the other significant purpose of the study. The spectral bands in the visible spectrum of MERIS were specifically designed for chl-a detection as is the case of other ocean color sensors such as the Sea-viewing Wide Field-of-view Sensor (SeaWiFS) and Moderate Resolution Imaging Spectroradiometer (MODIS), but the advantage of MERIS is an increased spatial resolution. The finer pixel size (300 m) of MERIS data is expected to retain details of some small scale phenomena, such as eddies and meanders, that might be lost with coarser spatial resolutions (over 1,000 m) of SeaWiFS and MODIS.

Material and Methods

Optical and chl-a data from 17 stations (Figure 1) collected on 4–6 December 2003 (Matsumura et al. 2006) were applied for the validations of remote sensing reflectance just above the sea surface ($R_{rs}(0+)$) (Eq. 1) and estimated chl-a.

$$R_{rs}(0+) = 0.519 \left(\frac{L_u(0-)}{E_d(0-)} \right), \quad (1)$$

where $E_d(0-)$ and $L_u(0-)$ are downward irradiance and upward radiance just below the sea surface, respectively—both measured in situ by using a Profiling Reflectance Radiometer model 600 (PRR-600). The instrument is capable of measuring profiles with 7 channels, each of which has 10 nm bandwidth (Table 1). Due to surface roughness, $E_d(0-)$ and $L_u(0-)$ were consequently obtained by extrapolating data

from 1 to 5 m depth (Matsumura et al. 2006). The constant 0.519 in Eq. 1 was derived from the downward Fresnel irradiance transmittance across the air-sea interface (0.96) (Mueller et al. 2003) and the upward radiance transmittance of the sea surface for normal incident (0.54) (Lubac and Loisel 2007). It plays a significant role to transform R_{rs} from just below (0-) to just above the sea surface (0+).

Water samples for chl-a analysis were collected and filtered (GF/F) onboard. The filtered papers were then stored in a freezer for further analyses in the laboratory by using chlorophyll fluorescence method following Strickland and Parson (1972). Chl-a was extracted from the filter remnant after adding 90% acetone, stirring vigorously, and centrifuging at 3,700 rpm for 5 min. The supernatant solution was extracted and measured for chl-a by using a fluorometer.

Table 1. Summary of the capabilities for electromagnetic detections of PRR-600 and MERIS in visible region.

PRR-600		MERIS in visible region	
Band center (nm)	Bandwidth (nm)	Band center (nm)	Bandwidth (nm)
412	10	412.5	10
443	10	442.5	10
490	10	490	10
520	10	510	10
565	10	560	10
—	—	620	10
670	10	665	10
683	10	681.25	7.5

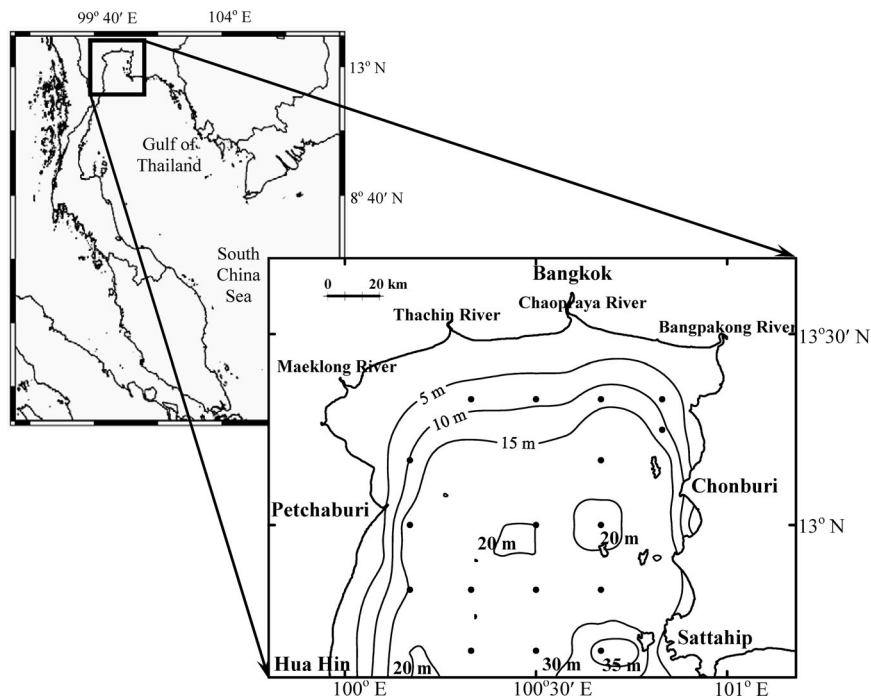


Fig. 1. The upper Gulf of Thailand. Contour lines represent water depth in meters and dots stand for observation points for optical and oceanographic data collections.

MERIS Level 2 (L2) products, atmospherically, radiometrically, and geometrically corrected (Antoine and Morel 1999), was used in this study. Two chl-a products, *algal_1* and *algal_2*, were also included in MERIS L2. *Algal_1* was estimated using empirical algorithm (MERIS-C) applied to normalized water reflectance after atmospheric correction (Morel and Antoine 2000), while *algal_2* was based on a radiative transfer model derived by using a neural network algorithm (Buckton et al. 1999). Chl-a estimated by the application of a local in-water algorithm, named Chula algorithm (Eq. 2) (Matsumura et al. 2006), on MERIS R_{rs} data, from now referred as *Chula_chl-a*, was also taken into consideration.

$$C_a = 181.4 \exp(-4.74 \cdot R_a) \quad (2)$$

$$R_a = \frac{R_{rs}(520)}{R_{rs}(565)}.$$

Where C_a is chl-a concentration (mg m^{-3}); $R_{rs}(520)$ and $R_{rs}(565)$ are remote sensing reflectance at wavelengths of 520 nm and 565 nm, respectively. All these three chl-a products were compared with the measured values to figure out the best estimated results for investigating surface chl-a distributions. Data in full mode resolution has a pixel size at nadir of 300 m, swatch area of 1,150 km, global coverage of 3 days, and a revisit period of 35 days (IOCCG, 1998). The MERIS data were provided by the European Space Agency (ESA). Basic ERS & Envisat AATSR and MERIS (BEAM) software was used to embed Chula algorithm on MERIS data, extract satellite data for validation, and mask land and cloud areas. This software is provided by ESA, which is available at <http://www.brockmann-consult.de/beam/index.html>.

Validations of Estimated Chl-a

This section presents evaluation results of standard MERIS chl-a products, including *algal_1* and *algal_2*, and *Chula_chl-a*. Due to the dynamic nature of the coastal water, only MERIS data collected at the same time as the field observations were used for verification purposes. The study area, which is located in the tropics, has almost continuous cloud cover. Subsequently, data collected on 4–6 December 2003, only one of six cruises conducted from October 2003 to July 2005 (Matsumura et al. 2006), were closely synchronized with a largely cloud free satellite overpass (5 December 2003). Data from a three-by-three pixel window centered on each sampling station were averaged and used for the analyses in order to minimize the effect of small scale variability of chl-a distribution.

MERIS R_{rs} data were investigated for their consistency prior to the application of the Chula algorithm for chl-a estimation because band centers in the visible regions of MERIS

are not identical to those of the PRR-600 (Table 1). Although the band centers of MERIS are not exactly the same as those of PRR-600, the bandwidth of 10 nm of most channels provides sufficient overlap. They are, therefore, assumed to be equivalent, and Chula algorithm could be directly applied to MERIS data without any modification. MERIS reflectance centered on 510 and 560 nm were validated with in situ data at wavelengths of 520 and 565 nm, respectively. These two bands and their ratios were selected to test because of their contribution to Chula algorithm. All validation results of MERIS R_{rs} and ratios are illustrated in Fig. 2. The normalized standard error of estimation ($Nor. S_{est}$) (Eq. 3) was introduced for comparison of the R_{rs} and the band ratios.

$$Nor. S_{est} = \sqrt{\frac{\sum (X_{cal} - X_{obs})^2}{n-1}} / \bar{X}_{obs}, \quad (3)$$

where X_{cal} and X_{obs} are calculated and observed values respectively; \bar{X}_{obs} is the means of observed values; and n is the number of observations.

MERIS R_{rs} were overestimated, observed from scattered points over the orthogonal lines (Figure 2 upper and middle

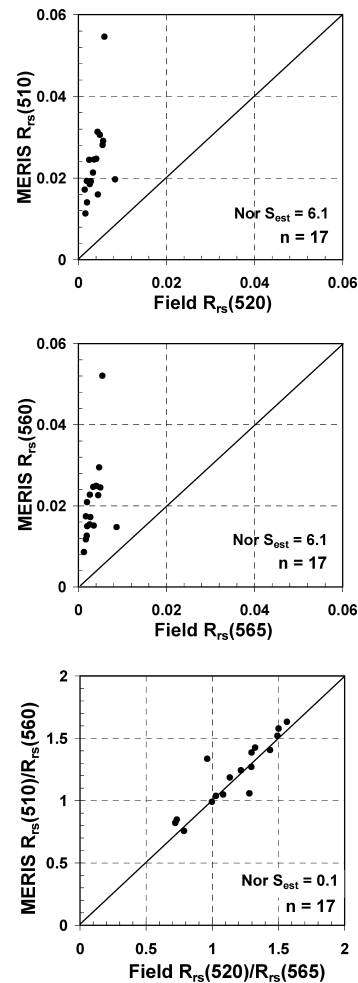


Fig. 2. Validations of $R_{rs}(510)$, $R_{rs}(560)$ and their ratios of MERIS data detected.

panels). This corresponds to relatively high $Nor: S_{est}$ of 6.1 in both cases. Improved results were observed when using R_{rs} ratios (Figure 2 lower panel); $Nor: S_{est}$ was reduced to 0.1 along with a reduction in scatter. Overestimation of R_{rs} may be originated from atmospheric path radiance effects on the surface reflectance. Given the consistency of the effects of the atmosphere between 510 and 560 nm, the ratios of R_{rs} tend to normalize for atmosphere. It is also realized that the overestimation in each spectral region can be generated by incomplete atmospheric correction over the Case 2 water (IOCCG 2000). This supports the use of ratios rather than band reflectance data alone for the chl-a algorithms. The experiment also supports the idea that the MERIS R_{rs} ratio of $R_{rs}(510)/R_{rs}(560)$ could be integrated into the Chula algorithm without any modification. This assessment is based, however, solely on the results of one cruise. Further verification is needed to confirm the reliability over a broader range of conditions.

Calculated chl-a based on the MERIS Chula algorithm together with MERIS chl-a products were validated. Scatter plots of predicted and in situ chl-a (Figure 3) indicate that Chula algorithm yielded a more consistent and reliable result than both MERIS products, which consistently overestimated chl-a content, especially in low chl-a situations. Error resulting from *algal_1* may be caused by inappropriate application of the chl-a product, designed for Case 1 water, on this Case 2 water. Such an error was also reported in other studies, e.g., Kratzer et al. (2008). What the derivation of *algal_1* algorithm did not take data sampled from Case 2 water into consideration (Morel and Antoine 2000) may be the cause of error in the resulting chl-a product when it was applied for coastal waters. Error from *algal_2*, whose algorithm is based on the radiative transfer model and neural network system (Doerffer and Schiller 1997), may be generated by local variations in water properties including chl-a, SS and CDOM of the study area. It is expected if the study area is well-trained, the accuracy of estimated chl-a shall increase. These examinations suggest the necessity of local algorithm development. It is, however, clear that the estimated chl-a from the Chula algorithm is well correlated with measured data.

Statistical analyses of the validation results of three chl-a candidates are summarized in Table 2. The standard error of estimation (S_{est}) (Eq. 4) and % accuracy (Eq. 5) are used for evaluation.

Table 2. Accuracy assessment of chl-a products derived from MERIS data.

Cruise Date	MERIS Date	Variables	Mean±SD (mg/m ³)	S_{est}	% Accuracy±C.I.*
4–6 Dec 2003	5 Dec 2003	Field	2.28±3.39		
		<i>algal_1</i>	3.94±8.06	6.0	−7.6±118.6
		<i>algal_2</i>	3.09±3.37	3.3	23.9±58.7
		Chula_chl-a	1.23±1.72	2.2	71.2±23.1

* 95 % Confidence interval

$$S_{est} = \sqrt{\frac{\sum (X_{cal} - X_{obs})^2}{n-1}} \quad (4)$$

$$\%Accuracy = 100 \times \left(1 - \frac{|X_{cal} - X_{obs}|}{X_{obs}} \right) \quad (5)$$

The averaged percent accuracy with a 95% confidence interval is presented. The analyses confirm the improvement of chl-a prediction based on the Chula algorithm by significantly reducing S_{est} and increasing the predictive power in comparison to *algal_1* and *algal_2*. The examinations suggest that Chula algorithm provides accuracy from about 50%

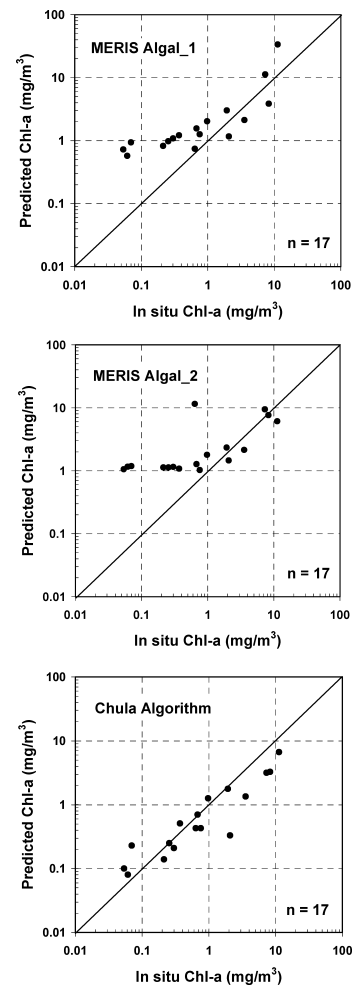


Fig. 3. Validations of estimated chl-a of MERIS *algal_1* and *algal_2* products and Chula algorithm.

to 90% in chl-a prediction with 95% confidence interval. MERIS data with the application of the Chula algorithm were, therefore, used for the investigation of surface chl-a distributions in UGoT. Due to the data limitations of this study, further testing researches should be conducted to verify the reliability of the algorithm under a broader range of conditions.

Surface Chl-a Distributions in UGoT

Chl-a maps of MERIS L2 data based on the Chula algorithm were produced to address chl-a distributions in the study area. Variations in monthly-mean wind directions

over UGoT averaged from 2003 to 2005 (QuickScat: <http://www.ssmi.com>) (Figure 4) were used to explain seasonal changes in the patterns of chl-a distributions. Only six relatively cloud free scenes were retrieved during cruise periods, from 2003 to 2005 (Figure 5). Among them, four scenes

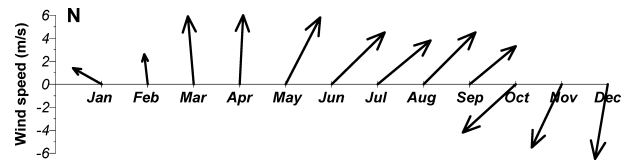


Fig. 4. Mean monthly wind vectors over UGoT averaged during 2003 and 2005 (Source: QuicScat, available at <http://www.ssmi.com>).

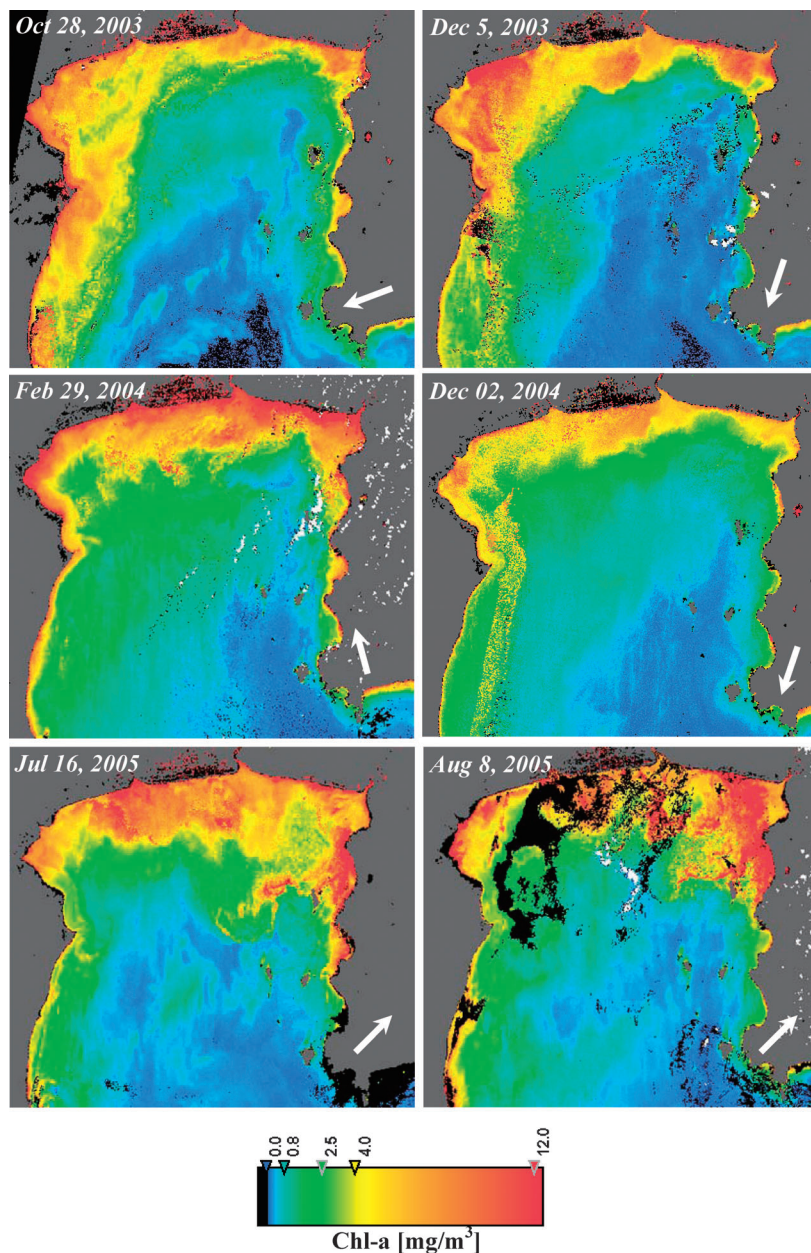


Fig. 5. Chl-a distributions in UGoT estimated by application of Chula algorithm on MERIS data. A white arrow in each image represents wind direction when the data was captured.

were imaged during the northeast or the southeast winds, and two scenes during the southwestern wind. Land and cloud were masked in dark gray and white colors, respectively.

Figure 5 shows chl-a to be quite high in the areas close to main river mouths in all seasons while changes in concentration corresponded to changes in prevailing wind directions (Figure 4). High chl-a bands migrated to the western coast when east or northeast winds prevailed over the area on October 28, 2003, December 5, 2003 and December 2, 2004. Chl-a accumulated near the northern coast when prevailing wind comes from the south on February 29, 2004. Low chl-a water along the eastern coast in those times suggests that there was a penetration of surface water from the central GoT to the east of UGoT. The chl-a patterns from July 16, 2005 and August 8, 2005 looks almost the same and may be used to represent the patterns of chl-a distributions during the southwest monsoon. A high chl-a band appeared along the northern coast including an accumulation in northeastern corner of UGoT in those times.

The temporal patterns of chl-a distributions in this study agree well with the population dynamics of a blooming plankton species reported in Sriwoon et al. (2008). This previous study also presented a series of monthly composite imaged of chl-a, acquired by SeaWiFS and MODIS, that the seasonal patterns are similar to our results. Application of finer spatial resolution of MERIS data in our study, however, significantly provides more details in chl-a distributions. It should be noted that, due to cloudiness problem, only six quality MERIS scenes were acquired. Small pattern of chl-a distribution, illustrated in this study, might be altered by abruptly changes in daily river discharge or wind just before satellite data collection.

The seasonal patterns of chl-a distribution presented corresponds to counter-clockwise and clockwise circulation develop during the northeast and the southwest monsoons, respectively (Buranapratheprat et al. 2002). High chlorophyll concentrations follow a similar pattern. This explains the seasonal and spatial distribution of red tides (Lirdwitayaprasit et al. 1994), as well as the coincidence of severe blooms during the wet season in the southwest monsoon (Piemsomboon 2003). Induced by southwest winds and eastward currents, large nutrient loads from river water accumulate in the northeastern corner of UGoT in wet season. Plankton blooms at this time become so intense that they commonly induce mass mortality of marine organism (Lirdwitayaprasit 1994). This is not the case during periods of northeast winds when dispersion, rather than accumulation, of nutrients following southwestward winds is noted. Resulting low incidence rates of blooming spread widely along the western coast. The understanding of seasonal dynamics of high chl-a areas can be used for coastal management to minimize severity of the problems resulting from plankton blooms in UGoT.

Conclusion

MERIS L2 data have been applied to the study of chl-a distributions in UGoT. MERIS R_{rs} overestimated in situ data but this error was reduced when R_{rs} ratios were applied. Estimated chl-a, derived from the use of the Chula algorithm to the MERIS data, was verified. Accuracy of this in-water algorithm for chl-a prediction exceeded those resulting from the application of the common MERIS algal_1 and algal_2 models. Chl-a maps, derived from the experiment, revealed that the patterns of chl-a distribution were related to seasonal wind fields. During the northeast monsoon high chl-a water moved westward, while during the southwest monsoon it moved in northeast corner of UGoT. These seasonal patterns of movement agree well with previous investigations on seasonal circulation and red tides in UGoT.

Acknowledgement

The authors would like to thank Dr. Mark Flaherty from University of Victoria, Dr. Kashane Chalermwat from Burapha University, and Dr. thaithaworn Lirdwitayaprasit from Chulalongkorn University for their supports; European Space Agency Envisat Project for providing MERIS data (Project ID 3426). The field campaigns were financially supported by the Japan Society for the Promotion of Science (JSPS), the Japan International Cooperation Agency (JICA) and the National Research Council of Thailand (NRCT). We also thank the two reviewers for their comments and suggestions.

References

- Antoine, D. and Morel, M. 1999. A multiple scattering algorithm for atmospheric correction of remotely sensed ocean color (MERIS instrument): principle and implementation for atmospheres carrying various aerosols including absorbing ones. *International Journal of Remote Sensing*, 20 (9), 1875–1916.
- Buckton, D., O'Mongain, E. and Danaher, S. 1999. The use of Neural Networks for the estimation of oceanic constituents based on the MERIS instrument. *International Journal of Remote Sensing*, 20 (9), 1841–1851.
- Buranapratheprat, A., Yanagi, T. and Sawangwong, P. 2002. Seasonal variations in circulation and salinity distribution in the upper Gulf of Thailand: modeling approach. *La Mer*, 40, 147–155.
- Cheevaporn, V. and Menasveta, P. 2003. Water pollution and habitat degradation in the Gulf of Thailand. *Marine Pollution Bulletin*, 47, 43–51.
- Chongprasith, P. and Srineth, V. 1998. Marine water quality and pollution of the Gulf of Thailand. pp. 137–204. *In*: D. M. Johnston (ed.) SEAPOL Integrated Studies of the Gulf of Thailand, Vol. 1. Southeast Asian Programme in Ocean Law, Policy and Management.
- Doerffer, R. and Schiller, H. 1997. Algorithm Theoretical Basic Document (ATBD), ATBD 2.12: Pigment Index, Sediment and Gelbstoff Retrieval from Directional Water Leaving Radiance Reflectances Using Inverse Modeling Technique. Available from

- http://envisat.esa.int/instruments/meris/atbd/atbd_2_09.pdf
- IOCCG. 1998. Minimum Requirements for an Operational Ocean-colour Sensor for the Open Ocean. *In*: A. Morel (ed.) Report of the International Ocean-Colour Co-ordinating Group. No. 1. IOCCG, Dartmouth, 50 pp.
- IOCCG. 2000. Remote Sensing of Ocean Colour in Coastal, and Other Optically-Complex, Waters. *In*: S. Sathyendranath (ed.) Report of the International Ocean-Colour Co-ordinating Group. No. 3, IOCCG, Dartmouth, 140 pp.
- Kratzer, S., Brockmann, C. and Moore, G. 2008. Using MERIS full resolution data to monitor coastal waters—A case study from Himmerfjärden, a fjord-like bay in the northwestern Baltic Sea. *Remote Sensing of Environment*, 112, 2284–2300.
- Lirdwitayaprasit, T., Vicharangsarn, T. and Sawetwong, N. 1994. Occurrences of red tide phenomena in the inner Gulf of Thailand during 1991–1994. *Proceeding of the First NRCT—JSPS Joint Seminar on Marine Science*. Chulalongkorn University Printing House, Bangkok, 106–110.
- Lirdwitayaprasit, T., Meksumpun, S., Rungsupa, S. and Furuya, K. 2006. Seasonal variations in cell abundance of *Noctiluca scintillans* in the coastal waters off Chonburi Province, the upper Gulf of Thailand. *Coastal Marine Science*, 30 (1), 80–84.
- Lubac, B. and Loisel, H. 2007. Variability and classification of remote sensing reflectance spectra in the eastern English Channel and southern North Sea. *Remote Sensing of Environment*, 110, 45–58.
- Matsumura, S., Siripong, A. and Lirdwitayaprasit, T. 2006. Underwater optical environment in the upper Gulf of Thailand. *Coastal Marine Science*, 30 (1), 36–43.
- Morel, A. and Antoine, D. 2000. Pigment Index Retrieval in Case 1 waters, MERIS Algorithm Theoretical Basis Document, ATBD2. Available from http://envisat.esa.int/instruments/meris/pdf/atbd_2_09.pdf
- Mueller, J. L., Morel, A., Frouin, R., Davis, C., Arnone, R., Carder, K. et al. 2003. Ocean optics protocols for satellite ocean color sensor validation, revision 4, volume III: Radiometric measurements and data analysis protocols. NASA Technical Memorandum. 2003-211621/Rev4-vol. III (p. 78). Greenbelt: NASA Goddard Space Flight Center.
- Piemsomboon, A. 2003. Influential factors on phytoplankton abundance and toxicity. pp. 43–54. *In*: ARRI (ed.) Red Tide Monitoring in the Gulf of Thailand. Aquatic Resources Research Institute, Chulalongkorn University and Water Quality Management Section, Pollution Control Department, Bangkok (in Thai).
- Rungsupa, S. 1997. Distribution pattern and density of *Noctiluca scintillans* around the upper Gulf of Thailand. *Kasetsart University Seminar: 22th February 1997*. 125–137.
- Silpipat, S. 1987. Circulation pattern in the upper Gulf of Thailand. *Proceedings of the Forth Seminar on the Water Quality and the Quality of Living Resources in Thai Waters: 7–9 July 1987*. National Research Council of Thailand, 82–93.
- Snidvongs, A. 1998. The oceanography of the Gulf of Thailand: Research and management policy. *In* SEAPOL Integrated Studies of the Gulf of Thailand, Vol. 1, ed. by D. M. Johnston, Southeast Asian Programme in Ocean Law, Policy and Management, 1–68.
- Sojisuporn, P. 1994. Density-driven and wind-driven current in the upper Gulf of Thailand. *Proceedings IOC-WESTPAC 3rd International Scientific Symposium*, 374–385.
- Sriwoon, R., Pholpunthin, P., Lirdwitayaprasit, T., Kishino, M. and Furuya, K. 2008. Population dynamics of green *Noctiluca scintillans* (Dinophyceae) associated with the monsoon cycle in the upper Gulf of Thailand. *Journal of Phycology*, 44, 605–615.
- Strickland, J. D. H. and Parsons, T. R. 1972. A Practical Handbook of seawater analysis. Fishery Research Board of Canada, Ottawa, 310 pp.